Journal of Applied Research and Technology

www.jart.ccadet.unam.mx
Journal of Applied Research and Technology 16 (2018) 422-436

Original

# Co/SBA-15 modified with TMB in the degradation of phenol

H. Pérez-Vidal [a,*], M. A. Lunagómez [a], J.G. Pacheco [a], J.G. Torres-Torres [a], D. De la Cruz-Romero [a], I. Cuauhtémoc-López [a], J.N. Beltramini [b]

[a] *Academic Division of Basic Science, Autonomous University Juarez of Tabasco, Km. 1, Road Cunduacán-Jalpa de Méndez, A.P. 24, C.P. 86690, Cunduacán, Tabasco, México.*

[b] *ARC Centre of Excellence for Functional Nanomaterials, the Australian Institute for Bioengineering and Nanotechnology, School of Engineering. The University of Queensland, St. Lucia, QLD 4072, Australia.*

Received dd mm aaaa; accepted dd mm aaaa
Available online dd mm aaaa

**Abstract:** Mesoporous materials like SBA-15 offer excellent properties such as catalyst support adsorbent due to its textural characteristics and their surface chemistry. The main objective of this study was to support cobalt (20 % w) in the type ordered mesoporous material SBA-15 and expand the pore size with the introduction of a "blowing agent", such as 1,3,5-trimethylbenzene (TMB), to be evaluated in the degradation of phenol. By its physicochemical characterization, it was confirmed that this is an ordered mesoporous material with two-dimensional hexagonal structure (p6mm) with high specific area, narrow pore distribution and typical morphology of this material. The pore size of SBA-15 has been extended to 19 nm by the addition of cosolvent organic molecules (TMB) and the particle size of cobalt decreased from 18.8 nm in SBA-15 to 6.4 nm on average by supporting it in SBA-15 modified with TMB; this property seems to confer the material be more selective in the conversion of CO2, which is the reason why it has greater activity for the degradation of phenol.

*Keywords:* SBA-15, phenol, mesoporous materials, cobalt, trimethylbenzene

## 1. INTRODUCTION

The possibility of modifying the porous structure and increasing the diameter of the pores of the SBA-15 with the use of expanding agents that dissolve in the internal (hydrophobic) zone of the micelles represents great advantages in the design of new catalytic materials (Can, Akça, Yilmaz, & Üner, 2006). There is the possibility of modifying its porous structure and increasing the diameter of the pores of the solid with the use of expanding agents that dissolve in the internal (hydrophobic) zone of the micelles, which represents great advantages in the design of new catalytic materials (Can et al., 2006). To increase the pore size there are publications that point to various methods such as the addition of salts, the use of co-surfactants, controlling the hydrothermal treatment, modifying the synthesis temperature, etc. However, the textural properties are affected. There is a wide variety of organic auxiliaries, among these, are paraffin, aromatic compounds, and alcohols (Raman, Anderson,& Brinker, 1996).

* Corresponding author.
*E-mail address:* hermicenda.perez@ujat.mx (H. Pérez-Vidal).

Peer Review under the responsibility of Universidad Nacional Autónoma de México.

http://

An organic agent that has been studied to increase the pore size and obtain a porous structure with structural uniformity is trimethylbenzene (TMB). It is only in 1998 that we have the first publication where they use an organic expanding agent 1,3,5-trimethylbenzene (TMB) which is a non-polar reagent that acts on the hydrophobic core of the micelles and expands them, thus increasing the pore size of the final product between 5 and 30 nm (Arellano, Zurita, Sazo, de Navarro, & López, 2008; Stucky et al., 2007; Wang, Noguchi, Takahashi, & Ohtsuka, 2001; Zhao et al., 1998). It was found that this agent provides a linear increase in the pore dimensions as its concentration increases. However, it was also shown that the final arrangement of the porous structure may be less orderly than when this type of expander is not used (Comerford, Farmer, Macquarrie, & Breeden, 2012; Esparza, 2007).

Achieving this type of materials with larger pore sizes allows them to be used as catalyst supports. Mesoporous silicas have recently been studied in heterogeneous reactions as supports for metallic oxides such as cobalt, highlighting the effects of parameters such as catalyst loading, peroxymonosulfate concentration and the reaction temperature in the degradation of phenol (Saputra et al., 2012; Shukla, Sun, Wang, Ang, & Tadé, 2011). In recent years it has been shown that industrial processes generate organic waste that is toxic to aquatic life, pollute rivers and groundwater. Phenol, when reacted with the chlorine used in most countries for the treatment of drinking water, forms phenyl-polychlorinated compounds that are more toxic and more resistant to biodegradation than phenol itself. The Phenol and phenolic compounds are harmful from the human health; they can cause tissue detachment, necrosis, digestive delay, kidneys and liver damage. Furthermore, if the discharge is at very low concentrations, they are highly dangerous to aquatic life and transfer a particularly unpleasant smell and taste. Therefore, the complete elimination of phenol in wastewater is necessary before it is discharged into the natural water streams. The process of catalytic oxidation via humid has been shown to be efficient in the destruction of this pollutant by reducing the conditions of pressure and reaction temperature in the presence of the catalyst (Chindris et al., 2010; Massa, Ivorra, Haure, Cabello, & Fenoglio, 2007).

The effective elimination of this pollutant becomes a task to be carried out due to the increasingly stringent environmental laws and regulations. The phenolic compounds occupy a prominent place in the list of pollutants of the environmental protection agency (EPA) of the United States of North America, due to the high toxicity, the high chemical demand of oxygen and the low biodegradability of these organic compounds. For this reason, oxidation processes have emerged as interesting alternatives for the destruction of organic pollutants in industrial wastewater (Dohnal & Fenclova, 1995; Esplugas, Gimenez, Contreras, Pascual, & Rodríguez, 2002; Gogate & Pandit, 2004). In this work, we investigate the performance of cobalt supported in the mesoporous material SBA-15 and the effect of TMB as an organic expanding agent, in order to expand the pore size and obtain catalytic supports with improved surface and structural properties for the phenol degradation.

## 2. MATERIALS AND METHODS

### 2.1 CATALYSTS PREPARATION

The synthesis of SBA-15 was performed varying the previously reported in the literature (Flodström, & Alfredsson, 2003; Zhao et al., 1998). A typical synthesis procedure of SBA-15 has 2.5% weight of Pluronic 123 (1.92 g), 45 g of water, 30 g of 4M HCl and 4 g of Tetraethyl-orthosilicate (TEOS) as a source of silicon (Zhao et al., 1998).

To synthesize 5 grams of SBA-15, 9.6 g of Pluronic 123 were dissolved in 225 mL of distilled water at room temperature and 150 mL of 0.5 M $HNO_3$ were added. The solution was then heated to 35 °C and stirred at 600 rpm for 4 hours. Then 20 grams of TEOS were added as a silicon source, stirring at 900 rpm for one minute, after that, it was left in moderate agitation (600 rpm) for 24 hours. Then, the solution was placed in a stove at 80 °C for 72 hours for hydrotreating. Finally, the solid obtained was washed with abundant water until neutral pH, dried at 80 °C for one hour and then calcined at 500 °C for 6 hours (with a ramp of 2 °C/min). The support achieved was impregnated with the precursor of Co $(NO_3)_2 \cdot 6H_2O$ (20% w) through a technique of impregnation to volume, after this, it was left to dry at room temperature and calcined at 350 °C for 6 hours with a heating ramp at 2 °C/ minute, the catalyst was designated Co/SBA-15.

In order to increase the pore size, the information reported in the literature was slightly changed (Stucky et

al., 2007) and consisted of the following: 4.0 g of Pluronic was dissolved in 30 mL of distilled water and 120 g. $HNO_3$ 0.5 M was added (Stucky et al., 2007 used 2M HCl) in a polypropylene canister.

It was stirred at room temperature until the Pluronic was dissolved. Subsequently, the solution was heated to 35 °C and stirred at 600 rpm. After 2 hours 3.0 g of TMB was added and 2 hours later 8.5 g of TEOS. It was stirred vigorously for one minute at 900 rpm, then left in moderate agitation (600 rpm) for 24 hours. It was placed in a hermetically sealed jar in an oven at 80 °C for 72 h (Stucky et al., 2007). The product was washed with abundant distilled water until obtaining a neutral pH, filtered, dried at room temperature and calcined in air at 500 °C for 6 hours with a heating ramp of 2 °C/min.

To obtain the Co20/SBA-15 and Co20/SBA-$15_{TMB}$ catalysts, the impregnation was carried out with 20 % by weight of precursor salt (cobalt nitrate) by the impregnation method at pore volume, it was left at room temperature and it was calcined at a temperature of 350 °C for 6 hours with a heating ramp of 2 °C/min.

### 2.2 CHARACTERIZATION TECHNIQUES

The cobalt content was obtained by atomic absorption in a Spectrometer Analyst model 700 AA. The measurements of nitrogen adsorption were carried out by means of a static volumetric procedure in a Micromeritics Tristar II 3020. The measurements were made at the normal boiling temperature of $N_2$ (77 K at atmospheric pressure).

The calculation of the specific surface ($S_{BET}$) was made based on the BET method (Brunauer-Emmett-Teller). The total pore volume was determined from the amount adsorbed at a relative pressure of approximately 0.99. The pore size distribution was determined using the Barrett-Joyner-Halenda method (BJH). The degree of ordering of the mesoporous structure was estimated by X-ray diffraction (XRD) in a Model D8 Advance equipment of the Bruker brand using the monochromatic CuKα radiation. The infrared analysis was performed on a Perkin Elmer Precise equipment (Spectrum One FT-IR Spectrometer). The catalysts were studied by scanning electron microscopy with an Analytical Scanning Electron microscope model JSM-6010LA and by transmission electron microscopy with Tecnai G2F30 microscope, field emission cannon (Schottky-FEG), with an acceleration voltage of 300 kV. The local chemical analysis by energy dispersive X-ray spectroscopy (EDXS) was performed in an X-ray spectroscope by energy dispersion that is attached to the microscope using STEM-EDX. The materials were identified as: SBA-15, SBA-$15_{TMB}$, Co20/SBA-15 and Co20/SBA-$15_{TMB}$, where: 20 = % Co and TMB = 1,3,5, Trimethylbenzene.

### 2.3 PHENOL DEGRADATION

For the oxidation reaction of the phenol, a high-pressure reactor (Parr Instruments Co Ltd, IL), 300 mL of phenol of a 500 ppm solution and 300 mg of catalyst were used. The system was heated to the temperature reaction and pressurized with nitrogen and with continuous stirring of 750 rpm, time zero was defined when the pre-set conditions were reached (temperature, 160 °C and oxygen pressure at 10 bar). The reaction was performed for 180 min. The samples in the effluent were taken at intervals of 10 min through 1h, and the phenol content (C), intermediate content and Total Organic Carbon (TOC) were analyzed. Total Organic Carbon (TOC) of the samples was measured with a TOC 5000 Shimadzu Analyzer. The conversion of phenol for the different materials and the TOC was calculated using:

$$X_{phenol} = \frac{C_0 - C_{180}}{C_0} \times 100\ \%$$

$$X_{TOC} = \frac{TOC_0 - TOC_{180}}{TOC_0} \times 100\ \%$$

Where $TOC_0$ is Total organic carbon at t=0 (ppm), $C_0$ is the phenol concentration at t = 0 (ppm), $C_{180}$ is the phenol concentration at t=3 h of reaction (ppm), $TOC_{180}$ is Total organic carbon at t=3 h of reaction (ppm). So the selectivity was calculated according to following equation (Luck, 1999):

$$S_{CO_2} = \frac{X_{TOC}}{phenol} \times 100$$

The initial rate ($r_i$) was calculated from the phenol conversion as a function of time, using the following equation:

$$r_i = \left(\frac{phenol(\%)}{\Delta t m_{cat}}\right)\ ([pollutant]_i$$

Where, $\frac{\Delta_{phenol}(\%)}{\Delta t}$ is the conversion at initial time;

$[pollutant]_I$ = initial concentration of the pollutant and $m_{cat}$= mass of catalyst ($g_{cat}L^{-1}$).

The chromatographic system to be used with this experiment consists of a Perkin Elmer Model Clarus 580 Gas Chromatograph which has a flame ionization detector (FID). The injector temperature maintained at 200 °C and the detector temperature maintained at 275 °C. The injection volume was 1-μL. The column was a VF-1ms: with dimensions: 30 m × 0.25 mm × 0.25 μm. The oven temperature maintained at 180 °C. The carrier gas used was helium with 99.999% of purity.

## 3. RESULTS AND DISCUSSION

### 3.1 PHYSICAL-CHEMICAL CHARACTERIZATION

Figure 1 shows the results of high angle XRDs of the synthesized materials (Co20/SBA-15, Co20/SBA-$15_{TMB}$) and, it was verified by XRDs at a low angle (Figure not shown) the obtaining of the hexagonal phase in two dimensions (*6pmm*) characteristic of the SBA-15 support.

Catalysts impregnated with 20 % by weight of cobalt (Co20/SBA-15) and, calcined at 350 °C show 4 peaks at 2θ: 37°, 43°, 60° and 65.5° (JCPDS: 03-065-3103 (I) and 00-043-1003), which correspond to the $Co_3O_4$ phase, this coincides with that reported by other authors (Akça, 2006; Jia et al., 2011; Ohtsuka, Arai, Takasaki, & Tsubouchi, 2003; Martínez & López, 2006; Shukla et al., 2011; Wang et al., 2001). In the Co20/SBA-$15_{TMB}$ catalyst, the typical shoulder of the SBA-15 is not observed at 23°, which we can infer as a disorder in the ordered mesoporous structure due to the addition of TMB that causes phase change (mesocellular foam) as reported by other authors (Johansson, Córdoba, & Odén, 2009; Lettow et al., 2000; Schmidt-Winke et al., 1999).

The textural properties are summarized in Table 1, the specific surface area ($S_{BET}$) was determined by the Brunauer-Emmett-Teller method (BET) (Brunauer, Emmett, & Teller, 1938) and the BHJ method was used to determine the volume and distribution of pore size (Barret et al., 1951). SBA-15 was obtained under strongly acidic conditions (pH = 0.6) using a triblock copolymer (Pluronic 123). These conditions have been previously reported (Bagshaw, Prouzet, & Pinnavaia, 1995; Flodström, & Alfredsson, 2003; Fukuoka et al., 2003; Lee, & Cheon, 2001; Zhao et al., 1998; Ryoo, Joo, & Jun, 1999; Yamada, Zhou, Asai, & Honma, 2002).

Figure 2a shows the nitrogen adsorption-desorption isotherms ($N_2$) of SBA-15, SBA-$15_{TMB}$, Co20/SBA-15 and Co20/SBA-$15_{TMB}$ and, in Figure 2b we can see the diameter distribution of pore of the supports (SBA-15 and SBA-$15_{TMB}$). It is observed that the isotherms are of type IV with a hysteresis cycle type H1 (according to the IUPAC classification) typical of these materials, which reflects that they are compact packings of cylindrical pores in an orderly manner (Huo, Margolese, & Stucky, 1996; Kruk, Jaroniec, & Sayari, 1997; Sing, 1985; Thieme & Schüth, 1999). However, in the solid with TMB (SBA-$15_{TMB}$) the hysteresis loop is different: it is of type *H2*, which indicates that there are non-cylindrical pores known as pores in the form of an inkwell of McBain. This pore is characterized by the radius of the wider (spherical) cavity and the radius of its narrowest cavity (cylindrical capillary) (Everet & Sidney, 1958; Gregg, Sing, & Salzberg, 1967), in which the body is larger than the mouth, hence we have different pore diameter in the adsorption and desorption (Figure 3) with a wider pore diameter distribution (Leofanti, Padovan, Tozzola, & Venturelli, 1998).

When the TMB was added, the pore diameter and volume were increased, the values were 19 nm and 0.97 $cm^3/g$ respectively. The SBA-$15_{TMB}$ with a larger pore diameter had a higher pore volume, while the SBA-15 with the diameter of 6.9 nm provides a higher specific area of 835 $m^2/g$, this coincides with that reported in other studies that they use expanding agents to expand the pore size (Lettow et al., 2000; Wang et al., 2001), with TMB being the most common compound for increasing the pore size of SBA-15, (Calin, Galarneau, Cacciaguerra, Denoyel, & Fajula, 2010; Doadrio et al., 2004; Jaladi, Katiyar, Thiel, Guliants, & Pinto 2009; Shih-Yuan et al., 2011; Wang et al., 2001).Likewise, it is reported that with the addition of TMB a phase transition from hexagonal to a mesocellular foam occurs when the TMB/P123 ratio exceeds 0.3 (Schmidt-Winkel et al., 1999), the maximum theoretical value of the size of the pores before the phase transition is 12 nm, which has also been demonstrated experimentally (Lettow et al., 2000). This value has been exceeded in this study as reported by other authors who have used other swelling agents such as hexane in the presence of $NH_4F$ (Sun et al., 2005), where $NH_4F$ increases the hydrophilic volume of P123, also the use of heptane seems to efficiently expand the volume of the hydrophobic micelle, which results in larger pores (Johansson et al., 2009).

The addition of 20 % cobalt in the SBA-15 produces the reduction in the textural properties (Figure 2a). The volume of $N_2$ adsorbed at relative pressures P/Po > 0.4 suggests partial plugging of the porosity by large particles of cobalt ($Co_3O_4$). The characteristic of the isotherms of mesoporous systems is maintained as well as the distribution of the pores that show a unimodal distribution. The narrow porch size distribution is shown in SBA-15 and Co20/SBA-15 confirms the uniformity of the mesoporous system. These results coincide with what was previously reported in the literature (Chytil, Haugland, & Blekkan 2008; Zhao et al., 1998; Flodström, & Alfredsson, 2003; Impéror-Clerc, Davidson, & Davidson, 2000; Martínez, López, Márquez, & Díaz 2003; Newalkar & Komarneni, 2001; Ryoo, Ko, Kruk, Antochshuk, & Jaroniec, 2000; Zhang et al., 2006).

With the intention of obtaining additional information on the nature of the siliceous skeleton in the SBA-15, the infrared spectroscopy technique was used in a range of 4000-400 $cm^{-1}$. Figure 4 shows a peak at 3450 $cm^{-1}$, associated with adsorbed water. The absorption band that appears at 1635 $cm^{-1}$ corresponds to δ(HOH) physisorbed water (Busca 1996; Gomez-Cazalilla, Mérida-Robles, Gurbani, Rodríguez-Castellón, & Jiménez-López 2007; Li, Shi, Zhang, Xiong, & Yan, 2004; Posada, Giraldo, & Cardona, 2011; Xia & Mokaya, 2004). The 4 characteristic bands of the SBA-15 appear in the spectrum (Jin et al., 2004; Selvaraj et al., 2005; Martínez & Ruiz, 2002; Xiao 2005). Three of these bands correspond to vibrations of silicon-oxygen bonds and can be classified by the type of movement of the oxygen atom with respect to the silicon atoms in the beam, bending and stretching (Kirk, 1998; Shen et al., 2006).

In Figure 5, the absorption spectra of the FT-IR in the range of 4000-500 $cm^{-1}$ of the supports and catalysts are shown: SBA-15, $SBA\text{-}15_{TMB}$, Co20/SBA-15 and $Co20/SBA\text{-}15_{TMB}$ and, in Table 2 the frequencies λ ($cm^{-1}$) of them are indicated. In Figure 5, a small shoulder around 568 $cm^{-1}$ is seen, this signal is attributed to Co-O bonds, suggesting the presence of a small amount of cobalt oxide crystallites as previously reported (Shukla et al., 2011; Tsoncheva, Ivanova, Rosenholm, & Linden 2009). It is observed that when supporting the cobalt in the SBA-15 there is a displacement of the δ(Si-O-Si) band to 471 $cm^{-1}$. However, when we introduced the TMB the vibrations δ (Si-O-Si) originally present in the SBA-15 did not observe it, nor the one corresponding to the symmetrical vibrations at 803 $cm^{-1}$, which indicates the presence of trimethyl in the skeleton of silica, and we observe that there is a displacement of the band 1080 $cm^{-1}$ to 1091 $cm^{-1}$ and, when introducing the cobalt in this support the characteristic band to the flexion of the silanol groups (Si-OH) disappears, the above can be related to the transformation of Si-OH groups into Si-O-Si $(CH_3)_3$, as reported by Jia et al. (2011) in the silylation of Co/SBA-15 catalysts for its application the synthesis by Fischer Tropsch.

It was also observed that the effect of heat treatment led to the formation of Co-O-Si species during calcination and significantly inhibited Co leaching; these results coincide with Hu, Yang, and Dang (2011) where their results show that $Co_3O_4$ was the main cobalt species present both inside and outside the support; Therefore, a synergic effect between the textural properties and the active centers for the degradation of phenol is explained in our work.

The images obtained by electron microscopy scanning (SEM) in the support and in the catalysts are shown in Figure 6 (a, b and c). The morphology observed was the typical forms of SBA-15 such as fibers, spheres, rods and short bars of ~ 0.5-2 μm in length that coincide with that reported by other authors (Chao et al., 2002; Björk, 2013; Sierra, Mesa, Ramírez, López, & Guth 2004; Katiyar, Yadav, Smirniotis, & Pinto, 2006; Zhao, Sun, Li, & Stucky 2000) the morphology does not change when introducing 20% by weight of cobalt. However, we observe mainly amorphous particles when the support is modified with TMB and impregnated with cobalt. The different forms are related to the conditions of synthesis as mentioned by Van Grieken, Hernández, and Calleja, (2003), they observed that the speed of agitation is one of the main variables that control the size and morphology of the particles of the mesoporous materials and, mention that the variation of this parameter allows preparing mesoporous silica spheres with a narrow particle size distribution in the range of 200-700 μm (Van Grieken, et al., 2003).

In addition, according to Johansson (2009), the length and diameter of the particles can be influenced by variations in the concentration of hydrochloric acid (HCl). This is due to the effect of HCl on the hydrolysis of TEOS. A higher concentration of this acid increases the hydrolysis which generates fewer micelles that can adhere to each other and the final particle shape is thinner.

Simultaneously, the rapid rate of hydrolysis increases the rate of cylindrical micelle formation. Therefore, at the highest concentrations of HCl, the micelles are more elongated, narrower and more homogeneous in length compared to those synthesized with HCl of lower concentration. In this study, we used a lower concentration of acid (0.5 M) compared to the typical synthesis using 2M HCl (Zhao et al., 1998) and a constant agitation of 600 rpm, which seems to be related to the final morphology of the supports and obtained catalysts.

Figure 7 (a, b, c, d, e, f) shows transmission electron microscopy (TEM) images of SBA-15 (a and b), Co20/SBA-15 (c and d), and Co20/SBA15$_{TMB}$ (e and f). In the first image (a) a typical morphology of the SBA-15 is observed as "honeycomb", where the mouth of the pores can be seen and, in Figure 7 (b) the hexagonal arrangement of pores is distinguished, whose longitudinal direction is perpendicular to the plane of the image. We can appreciate the walls of the pores, which form channels distributed in parallel with each other. With these TEM images characteristic of the ordered mesoporous material, the hexagonal structure (*p6mm*) in two dimensions previously reported in the literature is confirmed (Impéror-Clerc et al., 2000; Saika, Srinivas, & Ratnasamy 2006; Shukla et al., 2011) and is according to the results of low angle XRDs. In the micrograph corresponding to the Co20/SBA-15 (e and d) catalyst, the presence of $Co_3O_4$ aggregates on the external surface observed in the form of small particles confined to the mesopores is observed, which coincides with that reported by other authors (Hu et al., 2011; Lu et al., 2004; Martínez et al., 2003; Martínez & López, 2006).

In the analysis of the catalysts by TEM (Figure 7c), it reveals that the mesoporous silica presents an ordered structure with hexagonal symmetry that is not possible to appreciate when modifying the support with TMB (Figure 7e). In Figures 7e and 7f corresponding to Co20/SBA-15$_{TMB}$, the Co particles disseminated heterogeneously on the silica matrix can be distinguished. The introduction of an expanding agent such as TMB in the case of mesoporous materials such as MCM-41 that use an ionic surfactant does not alter the cylindrical shape of the pores, however, when the tribloque PEO-PPO-PEO is used as a template (P123) in the synthesis of SBA-15, the hexagonal structure of cylindrical pores is maintained only for low concentrations of TMB, as the ratio of TMB/P123 increases, a phase change (mesocellular) and the morphology of the particles are obtained. is affected (Letow et al., 2000; Schmidt-Winkel et al., 1999), this can be seen in the micrographs corresponding to Figures 7e and 7f; the average size of the cobalt particles (Figure 8) was estimated at ~ 18.8 nm for SBA-15 and of the order of ~ 6.4 nm on average for Co20/SBA-15$_{TMB}$.

Figure 9a and 9b show the EDS spectra of the solids with 20 % by weight of cobalt in the support SBA-15 and SBA-15$_{TMB}$ respectively (Co20/SBA-15 and Co20/SBA-15$_{TMB}$). It is observed that the relative amount of the metals varies in the two materials because of the possible diffusion effect when changing the structure of the pure silica (SBA-15) by the addition of the swelling agent 1,3,5 TMB. The strong signals of Co can be clearly detected, which confirms the presence of this element, however, we observed that the theoretical load deposited in the supports by impregnation at pore volume was 20 % by weight and this by EDS we see that it is lower: 16.33 % in Co20/SBA-15 and 8.55 % in Co20/SBA-15$_{TMB}$. Proving thereby that the method of preparing the materials results in cobalt dispersed heterogeneously in the supports as can be seen in the micrographs corresponding to Figure 7 (c, d, e, and f).

### 3.2 CATALYTIC EVALUATION

The catalytic activity of the mesoporous material SBA-15 modified with 1,3,5 TMB and with 20 % by weight of cobalt (Co20/SBA15$_{TMB}$), in the degradation of phenol was compared with pure silica (SBA-15). In Figure 10 we observe the degradation of phenol as a function of time as an indicator of the activity of the materials that was carried out at 180 minutes. It is observed that the phenol conversion of the support (SBA-15) differs significantly from the materials SBA-15$_{TMB}$ and Co20/SBA-15. The order of the conversion curves coincides with the degradation capacity; the most active material was Co20/SBA-15$_{TMB}$. This seems to be related to the effect of the heat treatment that generated the formation of Co-O-Si species during the calcination and significantly inhibited the leaching of the Co, these results coincide with Hu et al. (2011) where their results show that the $Co_3O_4$ is the main cobalt species present both inside and outside the support; Therefore, a synergic effect between the textural properties and the active centers for the degradation of phenol is explained in our work.

Figure 11 shows the results of the total organic carbon (TOC) normalized as a function of time at 180 minutes of

the reaction. It also shows the conversion percentages of total conversion of organic compounds to $CO_2$ and $H_2O$. In the reference material (SBA-15), we can observe that at 120 minutes only reached 20 % oxidation and the degradation with Co20/SBA15$_{TMB}$ shows the highest values in total organic carbon that is 86%, this indicates that some intermediary by products were formed during the oxidation reaction. Studies on the degradation of phenol with Co/SBA-15 report that the catalyst by itself does not have a strong adsorption of phenol, however with Co/SBA-15-oxone (Saputra et al., 2012; Shukla et al., 2011), the concentration of phenol gradually decreased and the rate of degradation appeared to be constant and the elimination of 100 % phenol was achieved in 180 min. This high rate of degradation was due to the activation of peroxymonosulfate (PMS) to produce sulfate radicals for the oxidation of phenol in heterogeneous solutions by $Co_3O_4$. We only obtained 86% in the degradation of phenol with Co20/SBA15$_{TMB}$ catalyst; PMS was not used in oxidation experiments. Shukla et al. (2011) show that cobalt precursors significantly influence the activity of Co/SBA-15 catalysts. The catalysts derived from cobalt chloride and acetate have shown similar activities and would achieve 100 % elimination of phenol in 200 min. However, the reaction rate from cobalt nitrate (as in this work) was much slower, reaching 100 % elimination in 390 min (Shukla et al., 2011).

In this study, the fact of reaching 86 % of phenol oxidation catalytic reaction may be related to the metallic particle size since the size decreased when the TMB was added; in the Co20/SBA-15 material, a particle size of 18.8 nm was estimated which is much larger than in the Co20/SBA15$_{TMB}$ which was 6.4 nm on average. The addition of TMB as a swelling molecule promotes better catalytic properties in materials synthesized with 20 % Cobalt, which can be attributed to the fact that this molecule distorts the mesoporous structure to the extent of disappearing the hexagonal array as observed by XRD. This disorder, in addition to allowing the formation of larger diameter pores (Figure 2b), modifies the structure of the surface favoring the distribution of cobalt particles to a size of ~ 6.4 nm, this being the most active, and which generates an adequate metal-support interaction, which manifests itself in the greater activity of the catalysts synthesized with TMB and with 20 % cobalt weight.

As mentioned, the total oxidation of phenol was not achieved in the catalysts at 120 minutes of reaction and the number of intermediate by products (catechol, hydroquinone, benzoquinone, oxalic acid, maleic acid and formic acid), were identified by gas chromatography in the solution after the reaction. Only traces of hydroquinone (less than 2 ppm), catechol (less than 1 ppm), traces of maleic acid and oxalic were found in these intermediate products. Oxidation of hydroquinone decreases more slowly than in the case of catechol oxidation because dihydroxybenzene groups are oxidized through different pathways.

The proposed mechanism by which the oxidation reaction of phenol is carried out is by free radicals, which can be either a phenolic or a hydroxyl group. Oxidation of an aromatic group can begin with the activation of the oxygen molecule or the hydrocarbon molecule and oxygen can participate in the reaction as an adsorbed species on the surface of the catalyst or from the structure of the metal oxide. Phenol degradation reaction can be described as follows: during the first steps of the reaction, phenol is degraded to aromatic compounds (such as catechol, hydroquinone, and benzoquinone), what was observed in the color change of the solution. The latter intermediates such as maleic acid, oxalic acid, and formic acid were formed after the opening of the aromatic ring, causing the solution to become colorless. These intermediate products were mineralized to $CO_2$ and $H_2O$. The color of the solution at the end of the reaction was colorless; which indicates that the aromatic intermediates were no longer present in the solution, these results according to what was reported by other authors (Bhargava et al., 2006; Hu et al., 2011; Ohta, Goto, & Teshima, 1980).

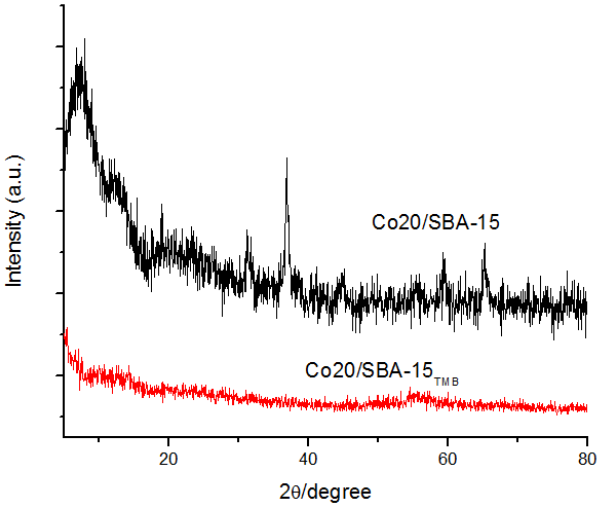


Fig. 1. XRD patterns for Co$_{20}$/SBA-15 and Co$_{20}$/SBA-15$_{TMB}$.

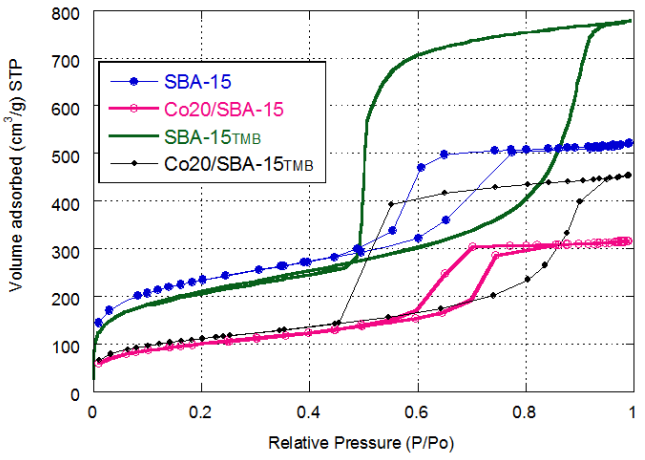


Fig. 2a. $N_2$ adsorption-desorption isotherms of SBA-15, Co20/SBA-15, SBA-15$_{TMB}$ and Co20/SBA15$_{TMB}$.

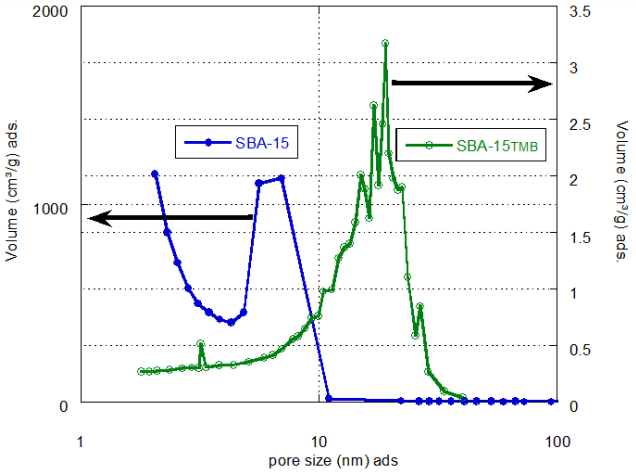


Fig. 2b. Pore size distribution of SBA-15 and SBA-15$_{TMB}$.

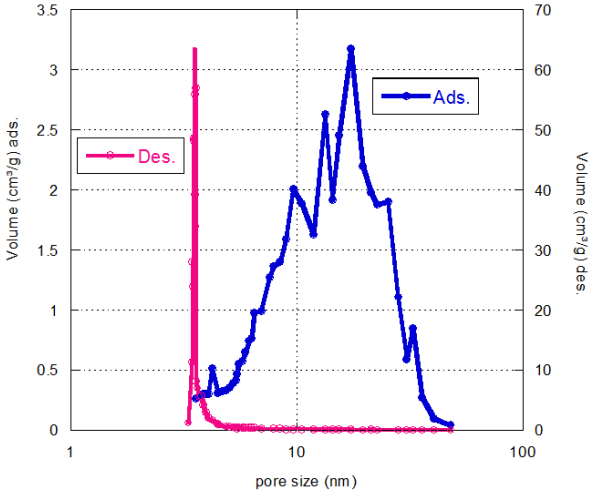


Fig. 3. BHJ pore volume distribution of SBA-15$_{TMB}$ sample, adsorption (Ads) and desorption (Des).

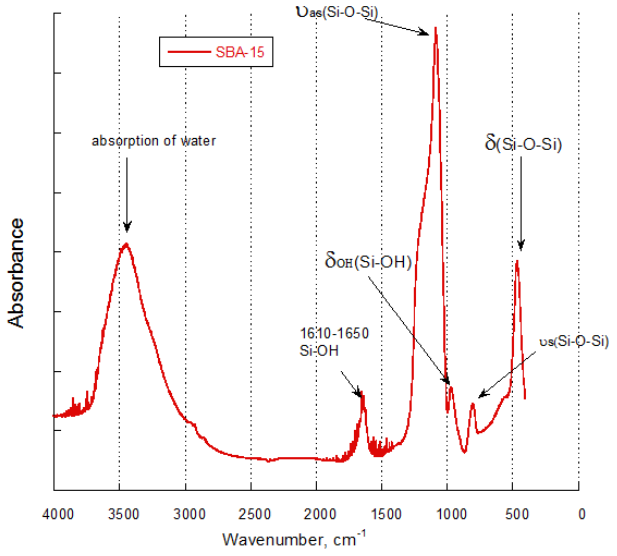


Fig. 4. FTIR absorption spectra in the 4000–400 cm−1 region of pure SBA-15.

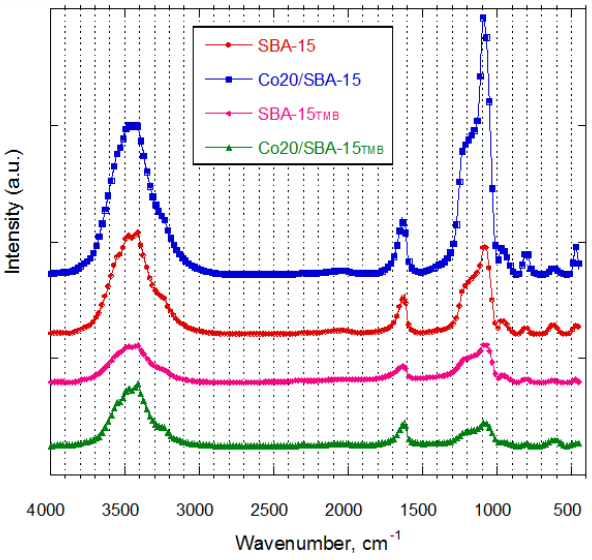


Fig. 5. FTIR absorption spectra in the 4000–400 cm$^{-1}$ region of pure SBA-15, SBA-15$_{TMB}$, Co$_{20}$/SBA-15 and Co$_{20}$/SBA-15$_{TMB}$.

In Table 3, the results of reaction rate (mmol h$^{-1}$), TOC, the percentage of conversion of phenol and the selectivity to $CO_2$ of the support and catalysts are shown. We can observe that the material Co20/SBA-15$_{TMB}$ presents the highest selectivity (93 %) as we can see in Figure 12. The conversion levels of phenol were higher when the Co was supported in the SBA-15 modified with TMB which is related to the smaller cobalt particle size and, the selectivity of the reaction towards complete mineralization was not observed in the synthesized materials.

Table 1. Textural properties (BET surface $S_{BET,}$ pore volume Vp, and pore diameter Dp) of SBA-15, $Co_{20}$/SBA-15, SBA-$15_{TMB}$ and $Co_{20}$/SBA$15_{TMB}$.

| Sample | $S_{BET}$ ($m^2/g$) | Vp ($cm^3/g$) | Dp* (nm)ads |
|---|---|---|---|
| SBA-15 | 835 | 0.70 | 6.7 |
| $Co_{20}$/SBA-15 | 356 | 0.50 | 7.6 |
| SBA-$15_{TMB}$ | 737 | 0.97 | 19.0 |
| $Co_{20}$/SBA-$15_{TMB}$ | 396 | 0.65 | 18.5 |

*Maximun value in the pore size distribution.

Table 2. Band assignment in the FTIR spectra of SBA-15 and Co-SBA-15X catalysts.

| Sample | λ ($cm^{-1}$) δ(Si-O-Si) | $\upsilon_s$(Si-O-Si) | $\delta_{OH}$(Si-OH) or υ(Si-O-M) | $\upsilon_{as}$(Si-O-Si) |
|---|---|---|---|---|
| SBA-15 | 479 | 803 | 967 | 1080 |
| $Co_{20}$/SBA-15 | 471 | 803 | 967 | 1083 |
| SBA-$15_{TMB}$ | --- | --- | 969 | 1091 |
| $Co_{20}$/SBA-$15_{TMB}$ | ---- | --- | --- | 1084 |

Table 3. Activity and selectivity for the catalyst Wet-Air Oxidation of phenol after 160 min of reaction.

| Catalysts | $r_1$[a] ($mmol\ h^{-1}$) | Abatement TOC (%)[a] | Phenol Conversion (%)[a] | Selectivity to $CO_2$[a] |
|---|---|---|---|---|
| SBA-15 | 0.9095 | 26 | 28 | 19 |
| SBA-$15_{TMB}$ | 0.9980 | 36 | 46 | 35 |
| Co20/SBA-15 | 1.663 | 60 | 58 | 42 |
| Co20/SBA-$15_{TMB}$ | 2.520 | 86 | 85 | 93 |

[a] Meassured after 120 min of reaction.

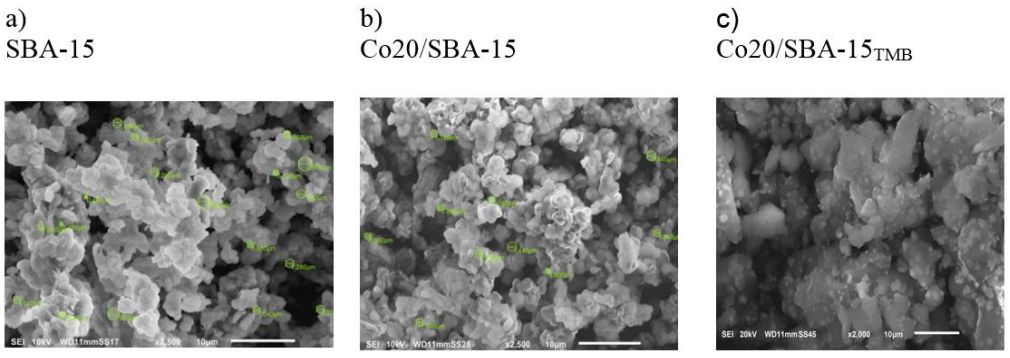


Fig. 6. Scanning electron micrographs (SEM) images of a) SBA-15, b) $Co_{20}$/SBA-15 and c) $Co_{20}$/SBA-$15_{TMB}$.

SBA-15

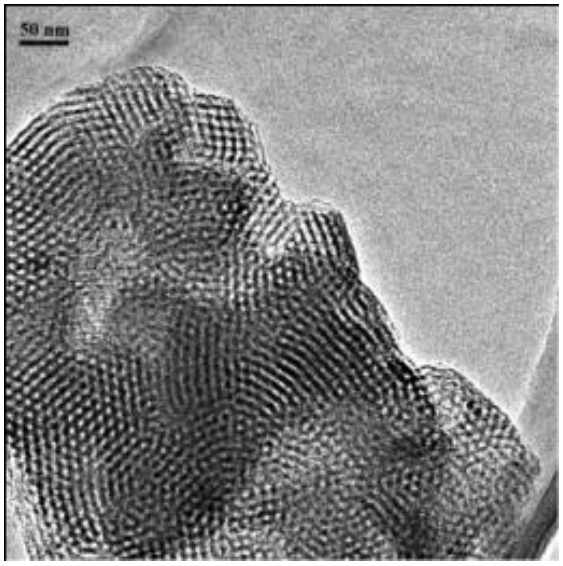


a)

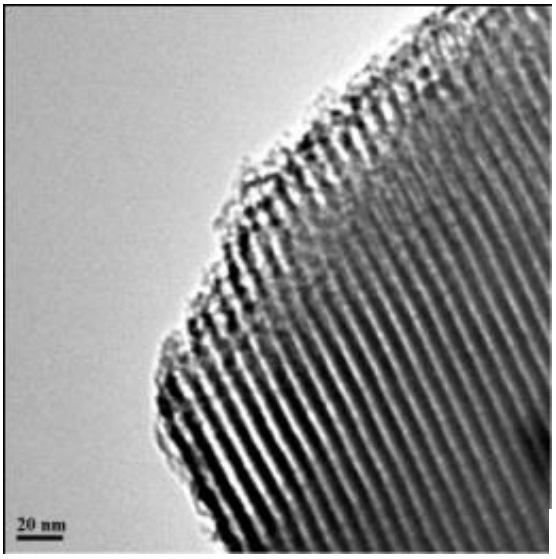


b)

Co20/SBA-15

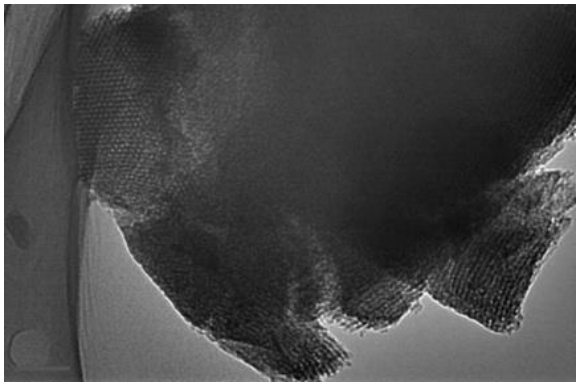

c)

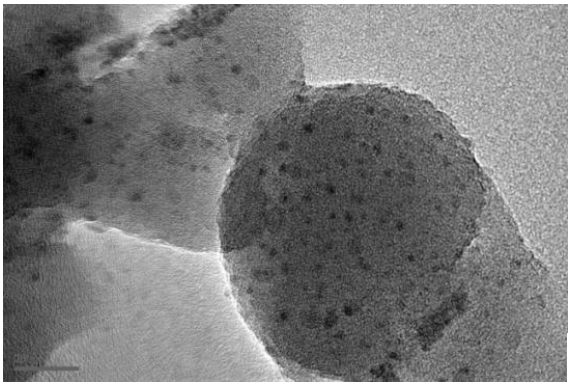

d)

Co20/SBA-15$_{TMB}$

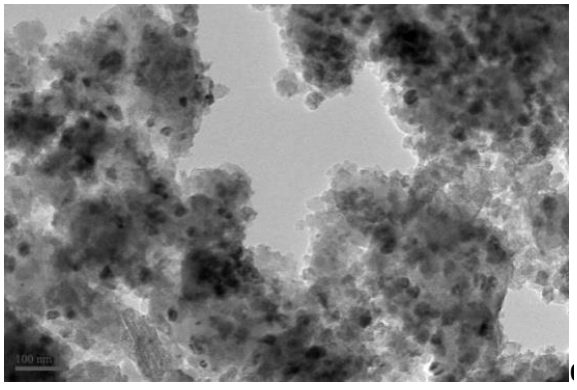

e)

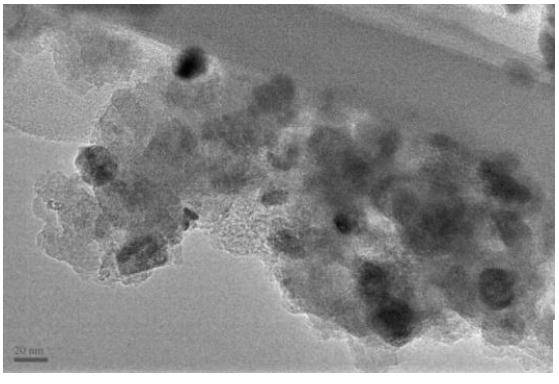

f)

Fig. 7. Transmission electron micrograph (TEM) images of sample SBA-15 (a and b), Co20/SBA-15 (c and d), Co20/SBA-15$_{TMB}$ (e and f).

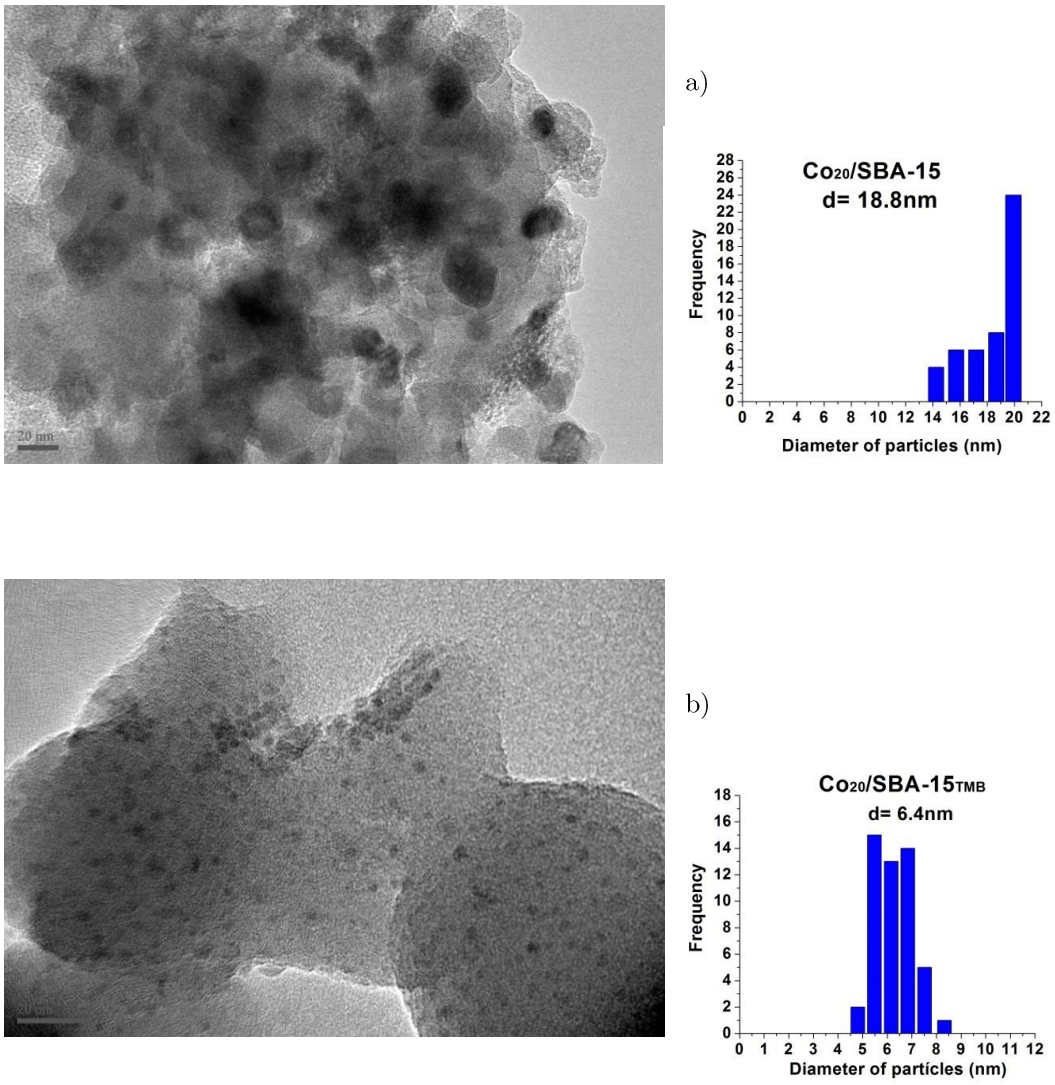


Fig. 8. TEM images a) Co20/SBA-15 and b) Co20/SBA-15TMB catalysts.

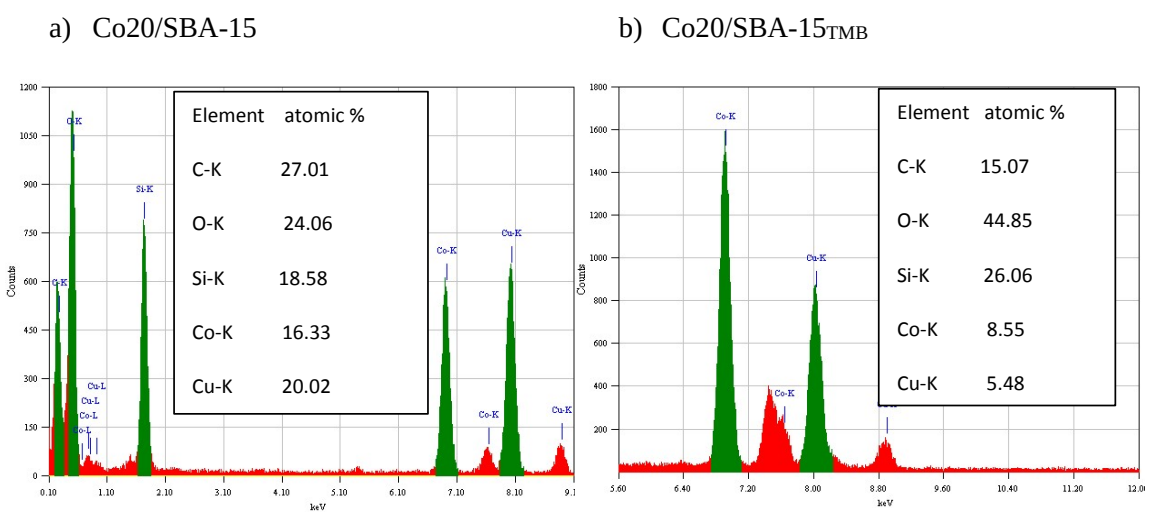


Fig. 9. EDS spectra of the solids: a) Co20/SBA-15 and b) Co20/SBA-15TMB.

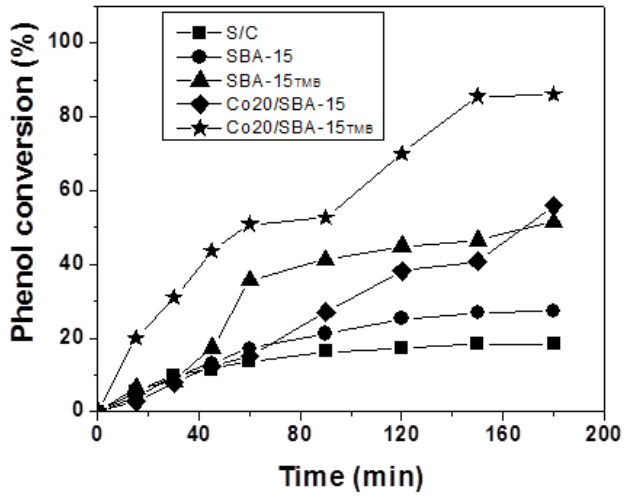


Fig. 10. Phenol conversions as a function of the time for SBA-15, SBA-15$_{TMB}$ and supported catalysts (T = 160°C, P $O_2$ = 10 bar).

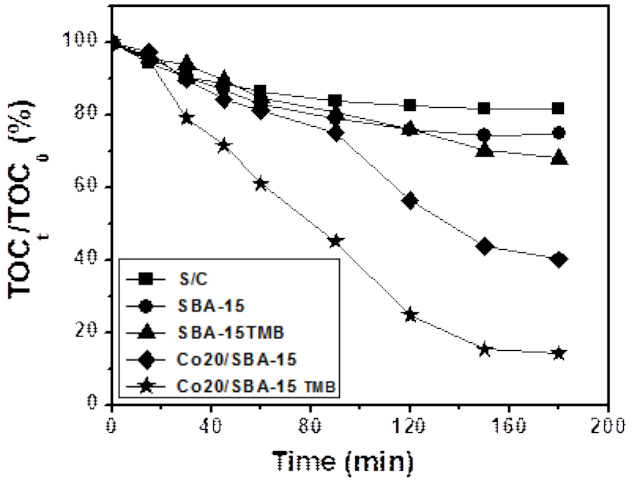


Fig. 11. TOC abatement as a function of the time for SBA-15, SBA-15$_{TMB}$ and supported catalysts.

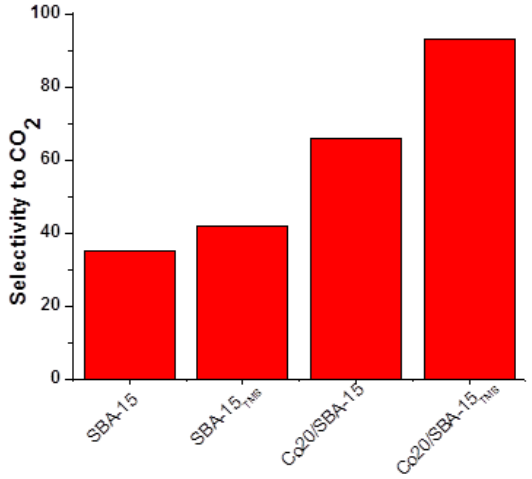


Fig. 12. Selectivity of SBA-15, SBA-15$_{TMB}$, Co20/SBA-15 and Co20/SBA-15$_{TMB}$ to $CO_2$.

## 4. CONCLUSIONS

The Co supported on the ordered mesoporous material SBA-15 and modified with 1,3,5 trimethylbenzene was found to be effective in phenol degradation. The modification of SBA-15 with the organic agent affected the textural, structural and catalytic properties of the synthesized materials, enlarged pore size and shape, changing the hysteresis loop from type I to type II indicating non-cylindrical pores and the average size of 19 nm in the SBA-15 modified with TMB.

The physical-chemical characterization of the support shows ordered structures of a mesoporous material two dimensions (*6pmm*) characteristic of the SBA-15 with the high specific area, narrow pore distribution and, when 20 % by weight of cobalt is supported, the textural properties and structural elements are maintained.

The morphology of the SBA-15 support is the typical one known as "honeycomb", and hexagonal structure of cylindrical pores and, when modifying the SBA-15 with TMB, there is a phase change (mesocellular) and the morphology of the particles. It is affected and the cobalt disperses heterogeneously in the support.

The addition of TMB expanded the pore size of the support, reducing the metallic particle size, this characteristic seems to give the material greater dispersion and be more selective in the conversion to $CO_2$, so that there is a greater activity for the degradation of phenol.

In Catalytic Wet Oxide Oxidation of phenol, the material of SBA-15 showed a degradation of 26 %, the catalyst with Co/SBA-15 reached 60 %. The Co20/SBA-15$_{TMB}$ catalyst obtained an oxidation of 86 % at 120 min of reaction. The effect of TMB on these catalysts was the increase in activity and selectivity to $CO_2$.

## ACKNOWLEDGMENTS

The first author is grateful and wishes to acknowledge the financial support of the Universidad Juárez Autónoma de Tabasco through the PFICA UJAT-2009-CO5-26 project.

## CONFLICT OF INTEREST

The authors have no conflicts of interest to declare.

## REFERENCES


Akça, B. U. R. C. U. (2006). *Synthesis and Characterization of Co-Pb/SBA15 Mesoporous Catalysts* (Doctoral dissertation, MS Thesis, Middle East Technical University, Ankara, Turkey).

Arellano, N., Zurita, M. J. P., Sazo, V., de Navarro, C. U., & López, C. (2011). Síntesis de sílices mesoporosas tipo SBA-15 a partir de un silicato de sodio de Venezuela. *Ciencia*, *16*(2).

Bagshaw, S. A., Prouzet, E., & Pinnavaia, T. J. (1995). Templating of mesoporous molecular sieves by nonionic polyethylene oxide surfactants. *Science*, *269*(5228), 1242-1244.

Barrett E. P., Joyner L. G., & Halenda P. P. (1951). The determination of pore volume and area distributions in porous substances. I. Computations from nitrogen isotherms, *Journal of the American Chemical Society, vol. 73* (1), pp. 373–380.

Bhargava, S. K., Tardio, J., Prasad, J., Föger, K., Akolekar, D. B., & Grocott, S. C. (2006). Wet oxidation and catalytic wet oxidation. *Industrial & engineering chemistry research*, *45*(4), 1221-1258.

Björk, E. M. (2013). *Mesoporous Building Blocks: Synthesis and Characterization of Mesoporous Silica Particles and Films*(Doctoral dissertation, Linköping University Electronic Press).

Brunauer, S., Emmett, P. H., & Teller, E. (1938). Adsorption of gases in multimolecular layers. *Journal of the American chemical society*, *60*(2), 309-319.

Busca, G. (1996). The use of vibrational spectroscopies in studies of heterogeneous catalysis by metal oxides: an introduction. *Catalysis today*, *27*(3-4), 323-352.

Calin, N., Galarneau, A., Cacciaguerra, T., Denoyel, R., & Fajula, F. (2010). Epoxy-functionalized large-pore SBA-15 and KIT-6 as affinity chromatography supports. *Comptes Rendus Chimie*, *13*(1-2), 199-206.

Can, M., Akça, B., Yilmaz, A., & Üner, D. (2006). Synthesis and characterization of Co-Pb/SBA-15 mesoporous catalysts. *Turkish Journal of Physics*, *29*(5), 287-294.

Chao, M. y H. L. (2002). *in: A. Sayari and M. Jaroniec (Ed.),* A study of morphology of mesoporous silica SBA15. *Studies in Surface Science and Catalysis, Elsevier.* Vol. 141. 387-394.

Chen, S. Y., Chen, Y. T., Lee, J. J., & Cheng, S. (2011). Tuning pore diameter of platelet SBA-15 materials with short mesochannels for enzyme adsorption. *Journal of Materials Chemistry*, *21*(15), 5693-5703.

Chindris A. (2010). Degradation of Refractory Organic Compounds in Aqueous Wastes employing a combination of biological and chemical treatments. Thesis. Cagliari: University of Cagliari.

Chytil, S., Haugland, L., & Blekkan, E. A. (2008). On the mechanical stability of mesoporous silica SBA-15. *Microporous and Mesoporous Materials*, *111*(1-3), 134-142.

Comerford, J. W., Farmer, T. J., Macquarrie, D. J., & Breeden, S. W. (2012). Mesoporous Structured Silica-An improved catalyst for direct amide synthesis and its application to continuous flow processing. *ARKIVOC: Online Journal of Organic Chemistry*.

Doadrio, A. L., Sousa, E. M. B., Doadrio, J. C., Pariente, J. P., Izquierdo-Barba, I., & Vallet-Regı, M. (2004). Mesoporous SBA-15 HPLC evaluation for controlled gentamicin drug delivery. *Journal of Controlled Release*, *97*(1), 125-132.

Dohnal, V., & Fenclova, D. (1995). Air-water partitioning and aqueous solubility of phenols. *Journal of Chemical and Engineering Data*, *40*(2), 478-483.

Esparza, S. J. M. (2007). *Estudio Experimental y Numérico de procesos desorción de $N_2$ en sólidos porosos modelo.*Tesis DOCTORAL para obtener el grado de doctor en ciencias (Química),UniversidadAutónomaMetropolitana,Méx.,D.F.

Esplugas, S., Gimenez, J., Contreras, S., Pascual, E., & Rodríguez, M. (2002). Comparison of different advanced oxidation processes for phenol degradation. *Water research*, *36*(4), 1034-1042.

Everet, D. H. & Sidney, S.F. (1958). Structure and Properties of Porous Materials;. *Colston Research Society.* Butter Worths Symposium, *London;* p10. 389 pp.

Flodström, K., & Alfredsson, V. (2003). Influence of the block length of triblock copolymers on the formation of mesoporous silica. *Microporous and mesoporous Materials*, *59*(2-3), 167-176.

Fukuoka, A., Sakamoto, Y., Araki, H., Sugimoto, N., Inagaki, S., Fukushima, Y., & Ichikaw, M. (2003). Template synthesis and catalysis of metal nanowires in mesoporous silicas. In *Studies in Surface Science and Catalysis* (Vol. 146, pp. 23-28). Elsevier.

Gogate, P. R., & Pandit, A. B. (2004). A review of imperative technologies for wastewater treatment I: oxidation technologies at ambient conditions. *Advances in Environmental Research*, *8*(3-4), 501-551.

Gómez-Cazalilla, M., Mérida-Robles, J. M., Gurbani, A., Rodríguez-Castellón, E., & Jiménez-López, A. (2007). Characterization and acidic properties of Al-SBA-15 materials prepared by post-synthesis alumination of a low-cost ordered mesoporous silica. *Journal of Solid State Chemistry*, *180*(3), 1130-1140.

Gregg, S. J., Sing, K. S. W., & Salzberg, H. W. (1967). Adsorption surface area and porosity. *Journal of the Electrochemical Society*, *114*(11), 279C-279C.

Hu, L., Yang, X., & Dang, S. (2011). An easily recyclable Co/SBA-15 catalyst: Heterogeneous activation of peroxymonosulfate for the degradation of phenol in water. *Applied Catalysis B: Environmental*, *102*(1-2), 19-26.

Huo, Q., Margolese, D. I., & Stucky, G. D. (1996). Surfactant control of phases in the synthesis of mesoporous silica-based materials. *Chemistry of Materials*, *8*(5), 1147-1160.

Imperor-Clerc, M., Davidson, P., & Davidson, A. (2000). Existence of a microporous corona around the mesopores of silica-based SBA-15 materials templated by triblock copolymers. *Journal of the American Chemical Society*, *122*(48), 11925-11933.

Jaladi, H., Katiyar, A., Thiel, S. W., Guliants, V. V., & Pinto, N. G. (2009). Effect of pore diffusional resistance on biocatalytic activity of Burkholderia cepacia lipase immobilized on SBA-15 hosts. *Chemical Engineering Science*, *64*(7), 1474-1479.

Jia, L., Jia, L., Li, D., Hou, B., Wang, J., & Sun, Y. (2011). Silylated Co/SBA-15 catalysts for Fischer–Tropsch synthesis. *Journal of Solid State Chemistry*, *184*(3), 488-493.

Jin, H., Wu, Q. & Wenqin, P. (2004). Preparation and conductivity of tungstovanadogermanic heteropoly acid supported on mesoporous silicate SBA-15. *Mater. Lett, 58, 29*, 3657-3660.

Johansson, E. M., Córdoba, J. M., & Odén, M. (2009). Synthesis and characterization of large mesoporous silica SBA-15 sheets with ordered accessible 18 nm pores. *Materials Letters*, *63*(24-25), 2129-2131.

Katiyar, A., Yadav, S., Smirniotis, P. G., & Pinto, N. G. (2006). Synthesis of ordered large pore SBA-15 spherical particles for adsorption of biomolecules. *Journal of Chromatography A*, *1122*(1-2), 13-20.

Kirk, C. T. (1988). Quantitative analysis of the effect of disorder-induced mode coupling on infrared absorption in silica. *Physical Review B*, *38*(2), 1255.

Kruk, M., Jaroniec, M., & Sayari, A. (1997). Application of large pore MCM-41 molecular sieves to improve pore size analysis using nitrogen adsorption measurements. *Langmuir*, *13*(23), 6267-6273.

Lee, K. B., Lee, S. M., & Cheon, J. (2001). Size-Controlled Synthesis of Pd Nanowires Using a Mesoporous Silica Template via Chemical Vapor Infiltration. *Advanced Materials*, *13*(7), 517-520.

Leofanti, G., Padovan, M., Tozzola, G., & Venturelli, B. (1998). Surface area and pore texture of catalysts. *Catalysis Today*, *41*(1-3), 207-219.

Lettow, J. S., Han, Y. J., Schmidt-Winkel, P., Yang, P., Zhao, D., Stucky, G. D., & Ying, J. Y. (2000). Hexagonal to mesocellular foam phase transition in polymer-templated mesoporous silicas. *Langmuir*, *16*(22), 8291-8295.

Li, L. I. A. N. G., Shi, J. L., Zhang, L. X., Xiong, L. M., & Yan, J. N. (2004). A Novel and Simple In-Situ Reduction Route for the Synthesis of an Ultra-Thin Metal Nanocoating in the Channels of Mesoporous Silica Materials. *Advanced Materials*, *16*(13), 1079-1082.

Lu, A. H., Li, W. C., Kiefer, A., Schmidt, W., Bill, E., Fink, G., & Schüth, F. (2004). Fabrication of magnetically separable mesostructured silica with an open pore system. *Journal of the American Chemical Society*, *126*(28), 8616-8617.

Luck, F. (1999). Wet air oxidation: past, present and future. *Catalysis today*, *53*(1), 81-91.

Martínez, A., López, C., Márquez, F., & Díaz, I. (2003). Fischer–Tropsch synthesis of hydrocarbons over mesoporous Co/SBA-15 catalysts: the influence of metal loading, cobalt precursor, and promoters. *Journal of Catalysis*, *220*(2), 486-499.

Martínez, A., & López, C. (2006). Catalizadores de Fischer-Tropsch basados en cobalto soportado sobre sílices mesoporosas ordenadas. *Revista Mexicana de Ingeniería Química*, *5*(3).

Martínez, J. R., & Ruiz, F. (2002). Mapeo estructural de sílica xerogel utilizando espectroscopía infrarroja. *Revista mexicana de física*, *48*(2), 142-149.

Massa, P., Ivorra, F., Haure, P., Cabello, F. M., & Fenoglio, R. (2007). Catalytic wet air oxidation of phenol aqueous solutions by 1% Ru/CeO2–Al2O3 catalysts prepared by different methods. *Catalysis Communications*,*8*(3),424-428.

Newalkar, B. L., & Komarneni, S. (2001). Control over Microporosity of Ordered Microporous– Mesoporous Silica SBA-15 Framework under Microwave-Hydrothermal Conditions: Effect of Salt Addition. *Chemistry of materials*, *13*(12), 4573-4579.

Ohta, H., Goto, S., & Teshima, H. (1980). Liquid-phase oxidation of phenol in a rotating catalytic basket reactor. *Industrial & Engineering Chemistry Fundamentals*, *19*(2), 180-185.

Ohtsuka, Y., Arai, T., Takasaki, S., & Tsubouchi, N. (2003). Fischer– Tropsch synthesis with cobalt catalysts supported on mesoporous silica for efficient production of diesel fuel fraction. *Energy & Fuels*, *17*(4), 804-809.

Posada, J. A., Giraldo, O. H., & Cardona, C. A. (2013). Síntesis y caracterización de sílicas mesoestructuradas funcionalizadas con grupos acidosulfónicos. *Revista Facultad de Ingeniería*, (58), 63-73.

Raman, N. K., Anderson, M. T., & Brinker, C. J. (1996). Template-based approaches to the preparation of amorphous, nanoporous silicas. *Chemistry of Materials*, *8*(8), 1682-1701.

Ryoo, R., Joo, S. H., & Jun, S. (1999). Synthesis of highly ordered carbon molecular sieves via template-mediated structural transformation. *The Journal of Physical Chemistry B*, *103*(37), 7743-7746.

Ryoo, R., Ko, C. H., Kruk, M., Antochshuk, V., & Jaroniec, M. (2000). Block-copolymer-templated ordered mesoporous silica: array of uniform mesopores or mesopore– micropore network?. *The Journal of Physical Chemistry B*, *104*(48), 11465-11471.

Saikia, L., Srinivas, D., & Ratnasamy, P. (2006). Chemo-, regio- and stereo-selective aerial oxidation of limonene to the endo-1, 2-epoxide over Mn (Salen)-sulfonated SBA-15. *Applied Catalysis A: General*, *309*(1), 144-154.

Saputra, E., Muhammad, S., Sun, H., Ang, H.M., Tade, M.O. & Wang, S. (2012). Red mud and fly ash supported Co catalysts for phenol oxidation.*Catalysis Today*, Vol. *190* issue 1, *68-72.*

Schmidt-Winkel, P., Lukens, W. W., Zhao, D., Yang, P., Chmelka, B. F., & Stucky, G. D. (1999). Mesocellular siliceous foams with uniformly sized cells and windows. *Journal of the American Chemical Society*, *121*(1), 254-255.

Selvaraj, M., Sinha, P. K., Lee, K., Ahn, I., Pandurangan, A., & Lee, T. G. (2005). Synthesis and characterization of Mn–MCM-41and Zr–Mn-MCM-41. *Microporous and Mesoporous Materials*, *78*(2-3), 139-149.

Shen, S., Chen, F., Chow, P. S., Phanapavudhikul, P., Zhu, K., & Tan, R. B. (2006). Synthesis of SBA-15 mesoporous silica via dry-gel conversion route. *Microporous and mesoporous materials*, *92*(1-3), 300-308.

Shukla, P., Sun, H., Wang, S., Ang, H. M., & Tadé, M. O. (2011). Co-SBA-15 for heterogeneous oxidation of phenol with sulfate radical for wastewater treatment. *Catalysis Today*, *175*(1), 380-385.

Sierra, L., Mesa, M., Ramírez, A., López, B., & Guth, J. L. (2004). Synthesis of micron-sized particles of mesoporous silica from tri-block surfactant in presence of fluorine, usable as stationary phases in HPLC. *Studies in Surface Science and Catalysis*, *154*, 573-580.

Sing, K. S. (1985). Reporting physisorption data for gas/solid systems with special reference to the determination of surface area and porosity (Recommendations 1984). *Pure and applied chemistry*, *57*(4), 603-619.

Stucky, D, G., Goleta, B. F., Chmelka, D. Z., Nick, M., Qisheng, H., Jianglin, F., Peidong, Y., David, P., David, M., Wayne, L. J.R., Glenn, H. F. & Patrick, Schmidt-Winkel. Block copolymer processing for mesostructured inorganic oxide materials. U. S. Patent No. 7,176,245. (2007).

Sun, J., Zhang, H., Ma, D., Chen, Y., Bao, X., Klein-Hoffmann, A., Pfänder, N. y Su, D. S. (2005). Alkanes-assisted low temperature formation of highly ordered SBA-15 with large cylindrical mesopores. *Chemical Communications*, (42), 5343-5345.

Thieme, M., & Schüth, F. (1999). Preparation of a mesoporous high surface area titanium oxo phosphate via a non-ionic surfactant route. *Microporous and Mesoporous Materials*, *27*(2-3), 193-200.

Tsoncheva, T., Ivanova, L., Rosenholm, J., & Linden, M. (2009). Cobalt oxide species supported on SBA-15, KIT-5 and KIT-6 mesoporous silicas for ethyl acetate total oxidation. *Applied Catalysis B: Environmental*, *89*(3-4), 365-374.

Van Grieken, R., Hernández, J. A. M., & Calleja, G. (2003). Síntesis y aplicación de materiales mesoestructurados: experiencia del Grupo de Ingeniería Química y Ambiental de la Universidad Rey Juan Carlos. In *Anales de la Real Sociedad Española de Química* (No. 4, pp. 31-42). Real Sociedad Española de Química.

Wang, Y., Noguchi, M., Takahashi, Y. & Ohtsuka, Y. (2001). Synthesis of SBA-15 with different pore sizes and the utilization as supports of high loading of cobalt catalysts. *Catalysis Today, 68(1-3)*, 3–9.

Xia, Y., & Mokaya, R. (2004). Ordered mesoporous MCM-41 silicon oxynitride solid base materials with high nitrogen content: synthesis, characterisation and catalytic evaluation. *Journal of Materials Chemistry*, *14*(16), 2507-2515.

Xiao, F. S. (2005). Ordered mesoporous silica-based materials templated from fluorocarbon–hydrocarbon surfactant mixtures and semi-fluorinated surfactants. *Current opinion in colloid & interface science*, *10*(3-4), 94-101.

Yamada, T., Zhou, H., Asai, K., & Honma, I. (2002). Pore size controlled mesoporous silicate powder prepared by triblock copolymer templates. *Materials letters*, *56*(1-2), 93-96.

Zhang, W. H., Zhang, L., Xiu, J., Shen, Z., Li, Y., Ying, P., & Li, C. (2006). Pore size design of ordered mesoporous silicas by controlling micellar properties of triblock copolymer EO20PO70EO20. *Microporous and mesoporous materials*, *89*(1-3), 179-185.

Zhao, D., Feng, J., Huo, Q., Melosh, N., Fredrickson, G. H., Chmelka, B. F., & Stucky, G. D. (1998). Triblock copolymer syntheses of mesoporous silica with periodic 50 to 300 angstrom pores. *science*, *279*(5350), 548-552.

Zhao, D., Sun, J., Li, Q., & Stucky, G. D. (2000). Morphological control of highly ordered mesoporous silica SBA-15. *Chemistry of Materials*, *12*(2), 275-279.